Supporting Information

Aminophosphonium organocatalysts for the ring-opening copolymerisation of epoxide and cyclic anhydride

Ella F Clark[a], Estelle Dunstan,[a] Gabriele Kociok-Köhn[b] and Antoine Buchard[c]

[a] Department of Chemistry, University of Bath, Bath, BA2 7AY, UK.

[b] Materials and Chemical Characterisation Facility, University of Bath, UK

[c] Department of Chemistry, University of York, York, YO10 5DD, UK.

E-mail : antoine.buchard@york.ac.uk

Contents

1 Materials and Methods

All reagents were purchased from Merck, Fischer Scientific, Alfa Aesar and Acros Organics. All solvents used were anhydrous unless otherwise stated. Anhydrous DCM and THF were purchased from Sigma Aldrich. Phthalic anhydride was stirred over hot anhydrous toluene overnight, filtered, then recrystallised twice from anhydrous toluene. Cyclohexene oxide was distilled four times under an argon atmosphere: firstly, stirring over CaH_2 and distilling, followed by stirring over Na and distilling finished with two additional distillations. (3-(Dimethylamino)propyl)triphenylphosphonium bromide was purchased from Apollo Scientific and used without further purification.

^{1}H, ^{13}C{^{1}H} and ^{31}P{^{1}H} spectra were recorded on a Bruker 400 or 500 MHz instrument or an Agilent 500 MHz instrument and referenced to residual solvent signals. Coupling constants are given in Hertz.

Mass spectrometry measurements were recorded with a microToF electrospray time of flight (ESI-ToF) mass spectrometer (Bruker Daltonik) in acetonitrile.

THF Size-exclusion chromatography (SEC) was carried out using a THF eluent and processed using multi analysis software. Polymer samples were dissolved at a concentration of 1 mg mL^{-1} in THF and analysed on an Agilent 1260 Infinity series instrument at 1 mL min^{-1} at 35 °C using two PLgel 5 μm MIXED−D 300 × 7.5 mm columns in series. Samples were detected with a differential refractive index (RI) detector. Number-average molar mass ($M_{n,SEC}$), and dispersities, ($Đ_M$ (M_w/M_n)) were calculated against a polystyrene calibration (11 polystyrene standards of narrow molar mass, ranging from M_w 615 - 568000 Da). Data was plotted using Origin 2023.

Matrix-assisted laser desorption ionization-time of flight (MALDI-ToF) mass spectrometry was conducted using a Bruker Autoflex speed MALDI Mass Spectrometer equipped with a 2 kHz Smartbeam-II laser. 40 mg of DCTB was dissolved in 1 mL of THF to prepare the matrix solution and 5 mg of sodium trifluoroacetate was dissolved in 1 mL of THF. 1 mg of poly(CHO-*alt*-PA) was dissolved in 1.0 mL of THF to prepare the polymer. The solutions were mixed in a matrix:polymer:sodium ratio of 4:1:4 respectively. 1 μL of the sample mixture were spotted on a 384 well ground steel MALDI target plate and left to dry before being

inserted into the MALDI instrument. Once loaded, positive ion MALDI spectra were obtained in linear mode. Laser intensity was varied. The data was analysed using the Flex Analysis software, version 3.4 (build 76). The molar mass distributions were obtained through analysis of the data in the Polytools software package 1.31.

In-situ FTIR analysis was done using a ReactIR 702L system from Mettler Toledo; measurements were recorded using a DiComp (Diamond) IR probe and TE MCT detector over a sampling range of 3000-650 cm^{-1}. The iC IR 7.1 Office software was employed to collect and process the data.

Single-Crystal X-ray Diffraction (XRD) analysis was carried out at 150(2) K on a Rigaku SuperNova, EosS2 single crystal diffractometer using monochromated CuKα radiation (λ = 1.5418 Å). Unit cell determination, data collection and data reduction were performed using the CrysAlisPro software. The structure was solved with SHELXT and refined by a full-matrix least-squares procedure based on F^2 (SHELXL-2018/3)[6]. All non-hydrogen atoms were refined anisotropically. Hydrogen atoms were placed onto calculated positions and refined using a riding model.

1.1 Synthesis of 1

Under argon atmosphere, bromine (198 µL, 3.88 mmol, 1 equiv.) was added dropwise to a solution of triphenylphosphine (1.02 g, 3.88 mmol, 1 equiv.) in anhydrous DCM (45 mL) at −78°C. After stirring for 2 hours at room temperature, a solution of N,N-dimethylethylenediamine (0.42 mL, 3.88 mmols, 1 equiv.) in DCM (1 mol L^{-1}) was added at −78 °C. After stirring overnight, the solvent was reduced and the product was precipitated from Et_2O, isolated *via* Buchner filtration. The product was then dried *in vacuo* at 40 °C to yield **1** (1.64 g, 99 % yield).

1.2 Synthesis of 2

Under argon atmosphere, bromine (198 µL, 3.88 mmol, 1 equiv.) was added dropwise to a solution of triphenylphosphine (1.02 g, 3.88 mmol, 1 equiv.) in anhydrous DCM (45 mL), at −78°C. After stirring for 2 hours at room temperature, a solution of benzylamine (0.42 mL, 3.88 mmol, 1 equiv.) and DABCO (217.6 mg, 1.94 mmol, 0.5 equiv.) in anhydrous DCM (2 mL) was added at −78°C to the mixture. After stirring overnight, the solvent was removed *in vacuo*, the product was redissolved in THF and any remaining solid was removed by centrifugation (2900 rpm, 5 minutes). The solvent

was then reduced, and the **3** was precipitated from Et_2O, isolated *via* Büchner filtration and dried *in vacuo* at 40°C. (1.07 g, 62 % yield).

1.3 Synthesis of 4

Under argon atmosphere, bromine (198 µL, 3.88 mmol, 2 equivs.) was added dropwise to a solution of triphenylphosphine (1.02 g, 3.88 mmol, 2 equivs.) in anhydrous DCM (45 mL) at −78°C. After stirring for 2 hours at room temperature, a solution of ethylenediamine (0.13 mL, 1.94 mmol, 1 equiv.) in DCM (1 mol L^{-1}) was added at −78 °C. After stirring overnight, the solvent was reduced and the product was precipitated from Et_2O, isolated *via* Buchner filtration. The product was then dried *in vacuo* at 40 °C to yield **4** (1.07 g, 94 % yield).

1.4 General Procedure for the ROCOP of CHO/PA

A typical procedure for copolymerisation of epoxides with cyclic anhydrides: In a glovebox, the catalysts (5 x 10^{-3} mmol), phthalic anhydride (0.148g, 1 mmol) and cyclohexane oxide (0.098 g, 2 mmol) were added into a 4 mL dram vial. The vial was sealed and heated using a DrySyn® heating block at 120 °C. After the allotted reaction time, the polymerisation was quenched with non-anhydrous $CDCl_3$. The polymer was precipitated from cold Et_2O and isolated *via* centrifugation (2900 rpm, 5 minutes) and the resulting polymer was dried *in vacuo* at 50 °C for 15 hours.

1.5 Synthesis of 1·HCl

1 (20 mg, 0.047 mmol, 1 equiv) was dissolved in $CHCl_3$ (1.6 mL). 23 µL of HCl solution (2 mol dm^{-3} in Et_2O, 0.047 mmol, 1 equiv) was added and the solution was stirred for one hour. The solvent was removed *in vacuo* and the resulting white powder dried overnight at 40 °C *in vacuo*, before being used in catalysis. The resulting product was analysed via NMR analysis in $CHCl_3$, which showed one signal at 39.00 ppm in $^{31}P\{^1H\}$ NMR, and an identical spectrum to **1** by ^1H NMR.

1.6 Density Functional Theory Calculations

DFT calculations were performed using Gaussian16 suite of codes (revision C.01).[1] Geometries were fully optimised without any symmetry or geometry constraints, and using an “ultrafine” grid for numerical integration, and using the hybrid exchange-correlation ωb97XD functional developed by Chai and Head-Gordon.[2,3] The 6-311++G(2d,p) basis set was used for O, P, Br and N atoms and the 6-31+G(d,p) was used for C and H atoms. All structures are optimized using the self-consistent reaction

field (SCRF) approach with conductor-like polarisable continuum model (CPCM) In polymerization reactions, the cyclohexene oxide (CHO) monomer also serves as the solvent but is not implemented as a standard solvent in Gaussian 16. THF was therefore use as a proxy. The identification of all the stationary points as minima or transition states as a first-order saddle point on the potential energy surface was confirmed through vibrational frequency calculations.

Free enthalpies were corrected using Goodvibes software,[4] with Grimme's quasiharmonic approximation applied with a frequency cut-off value of 100.0 wavenumbers, a frequency scale factor = 1.0. To account for experimental conditions, a temperature of 393.15 K and concentrations of 5.07 mol L–1 (for neat CHO), and 0.0127 mol L –1 (for any catalytic species) were also applied. All intermediates and transition states were characterised by normal coordinate analysis revealing either precisely zero or one imaginary frequency, respectively. In the case of transition states, the imaginary frequency corresponds to the mode of the intended reaction step.

Full coordinates for all structures, together with computed energies and vibrational frequency data, are available via the corresponding Gaussian 16 output files and calculation spreadsheet, stored in the open-access digital repository, DOI: 10.6084/m9.figshare.26487826

2 Characterisation data for 1

2.1 NMR spectroscopy analysis

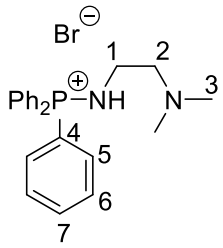

^{1}H NMR (500 MHz, $CDCl_3$, δ (ppm)): 7.79 (m, 9H, H-6, H-7), 7.68 (m, 6H, H-5), 3.57 (m, 2H, H-1), 3.38 (m, 2H, H-2), 2.67 (s, 6H, H-3)

^{13}C{^{1}H} NMR (126 MHz, $CDCl_3$, δ (ppm)):135.4 (d, *J* = 3.6 Hz, C-7) 133.8 (d, *J* = 14.2 Hz, C-6), 130.4 (d, *J* = 16.6 Hz, C-5), 121.0 (d, *J* = 128.7 Hz, C-4), 57.6 (C-2) 43.9 (C-3), 38.2 (C-1)

^{31}P{^{1}H} (202 MHz, $CDCl_3$, δ (ppm)): 39.15

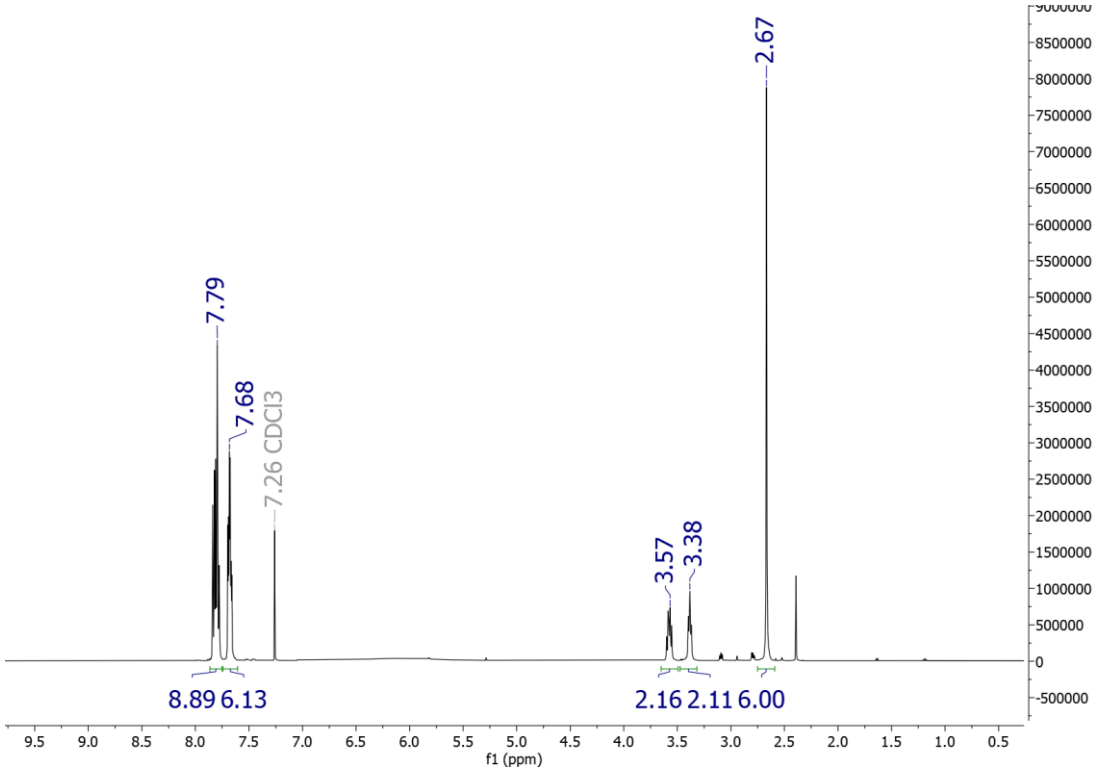

Figure S1. ^{1}H NMR spectrum of **1**.

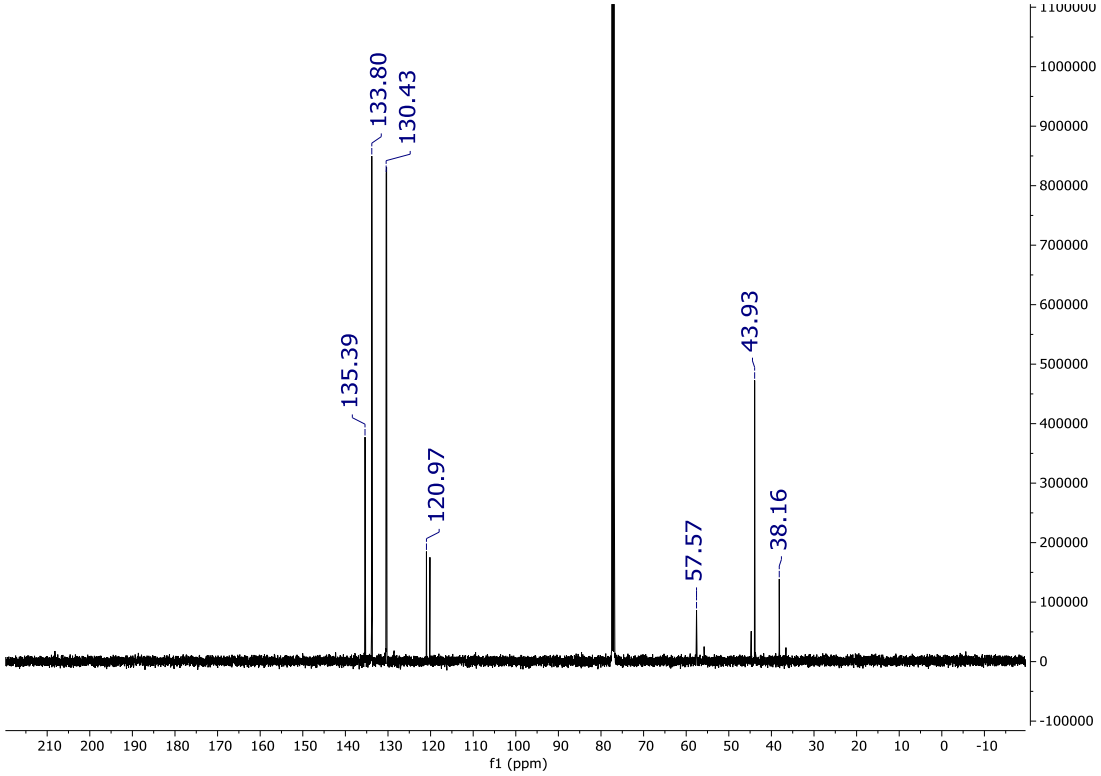

Figure S2. $^{13}C\{^{1}H\}$ NMR spectrum of **1**, residual $CDCl_3$ signal at 77.16 ppm.

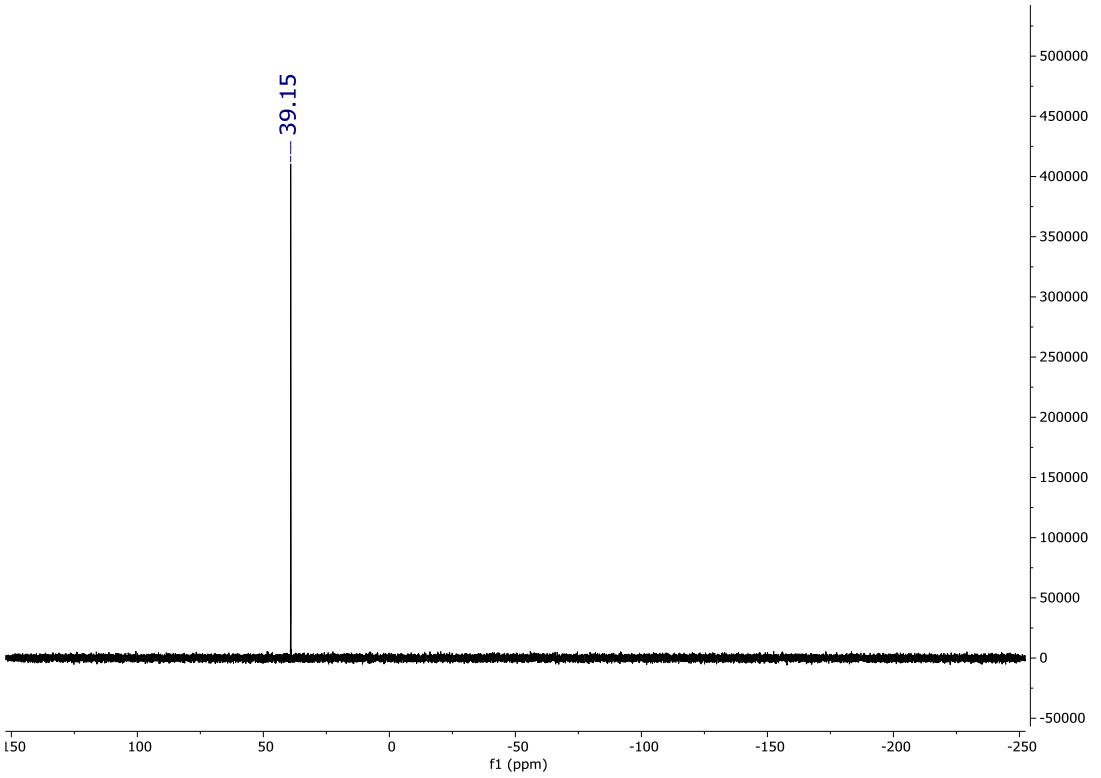

Figure S3. $^{31}P\{^{1}H\}$ NMR spectrum of **1**.

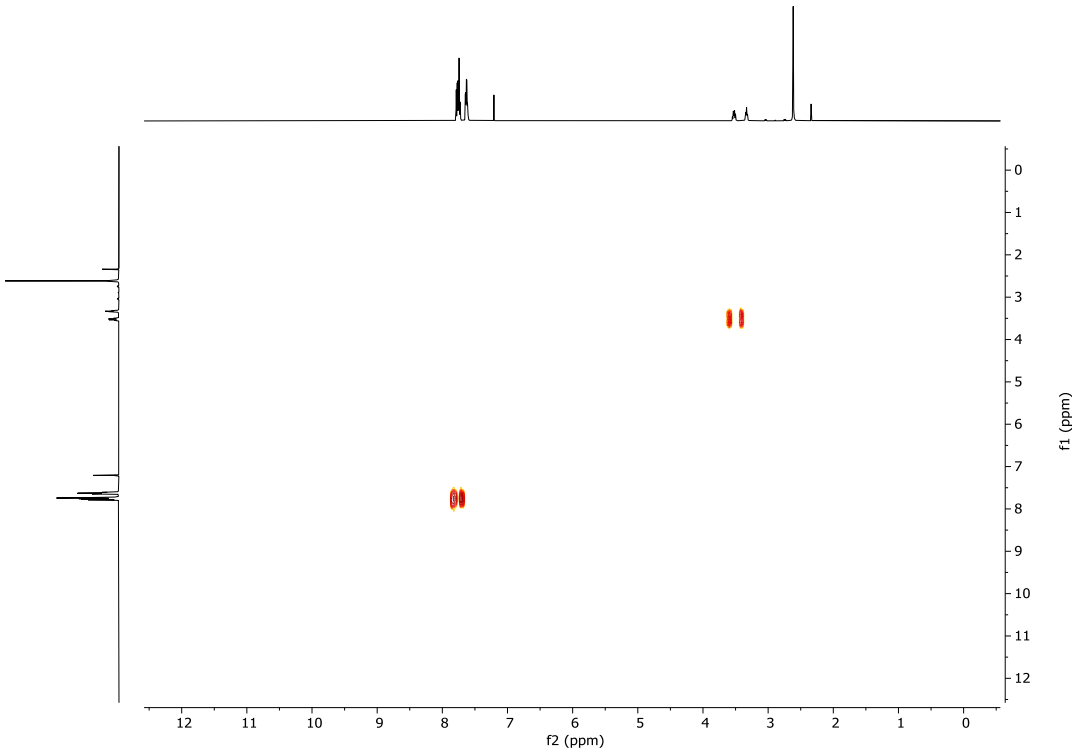

Figure S4. ^{1}H COSY NMR spectrum of **1**.

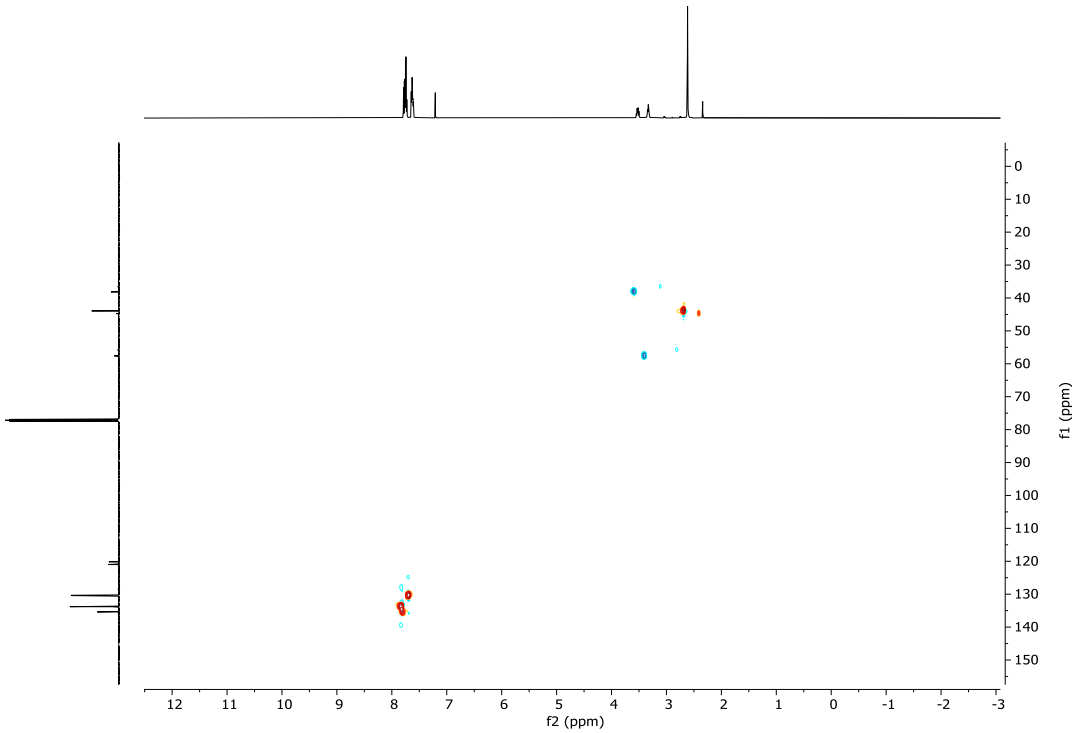

Figure S5. ^{1}H-^{13}C HSQC NMR spectrum of **1**.

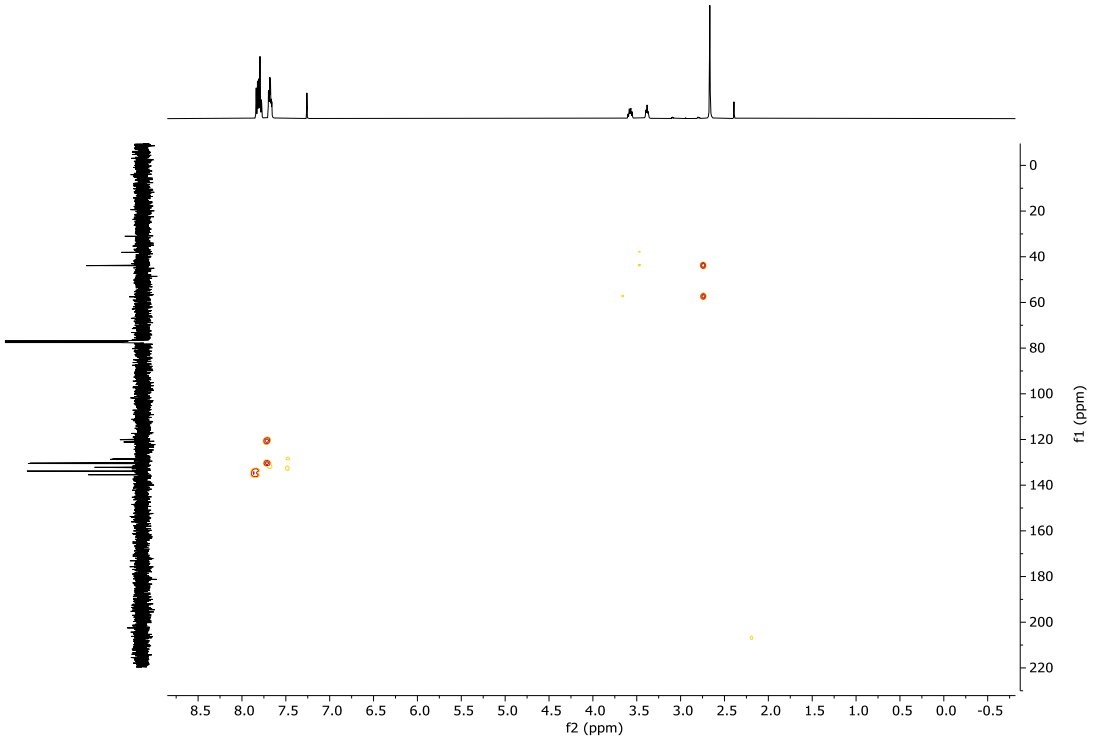

Figure S6. ^{1}H-^{13}C HMBC NMR spectrum of **1**.

2.2 X-ray diffraction analysis

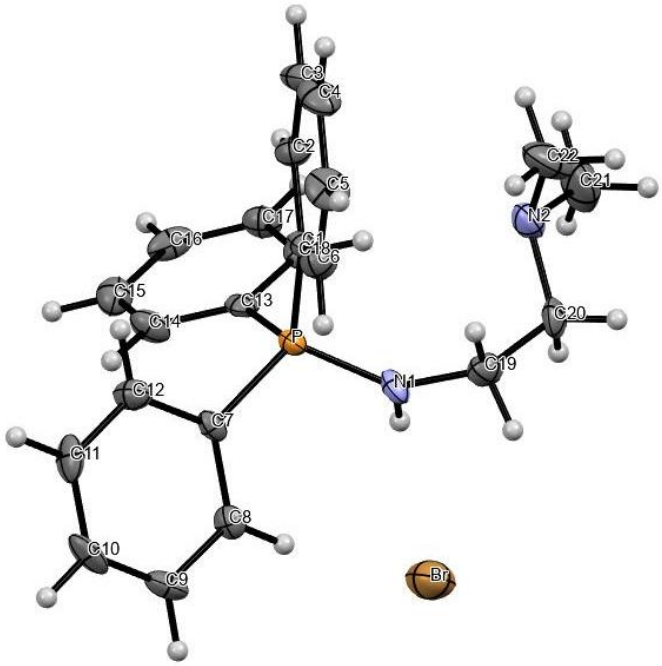

Figure S7. ORTEP drawing of the molecular structure of **1** obtained by X-ray diffraction analysis, with thermal ellipsoids at the 50% probability level. CCDC 2374662.

Identification code	e23ab7a
Empirical formula	C_{22} H_{26} Br N_2 P
Formula weight	429.33
Temperature	149.9(5) K
Wavelength	0.71073 Å
Crystal system	Monoclinic
Space group	$P2_1/c$
Unit cell dimensions	a = 9.4539(5) Å α = 90°.
	b = 16.8444(9) Å β = 109.865(7)°.
	c = 13.8253(8) Å γ = 90°.
Volume	2070.6(2) $Å^3$
Z	4
Density (calculated)	1.377 Mg/m^3
Absorption coefficient	2.071 mm^{-1}
F(000)	888
Crystal size	0.641 x 0.221 x 0.091 mm^3
Theta range for data collection	3.133 to 27.484°.
Index ranges	-12<=h<=12, -21<=k<=21, -17<=l<=17
Reflections collected	17883
Independent reflections	4729 [R(int) = 0.0375]
Completeness to theta = 25.242°	99.8 %
Absorption correction	Semi-empirical from equivalents
Max. and min. transmission	1.00000 and 0.74544
Refinement method	Full-matrix least-squares on F^2
Data / restraints / parameters	4729 / 1 / 241
Goodness-of-fit on F^2	1.048
Final R indices [I>2sigma(I)]	R_1 = 0.0494, wR_2 = 0.1427
R indices (all data)	R_1 = 0.0629, wR_2 = 0.1511
Extinction coefficient	n/a
Largest diff. peak and hole	0.768 and -0.990 $e.Å^{-3}$

2.3 Mass spectrometry analysis

Figure: Extracted ion chromatogram (EIC) of compound.

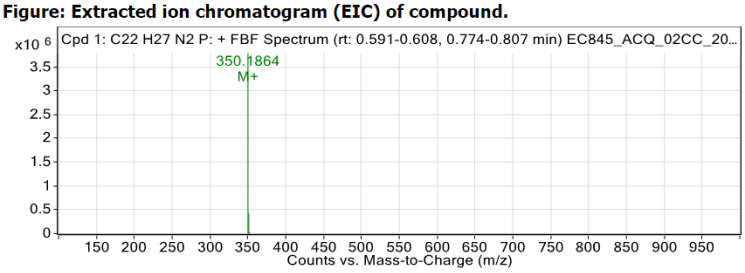

Figure: Full range view of Compound spectra and potential adducts.

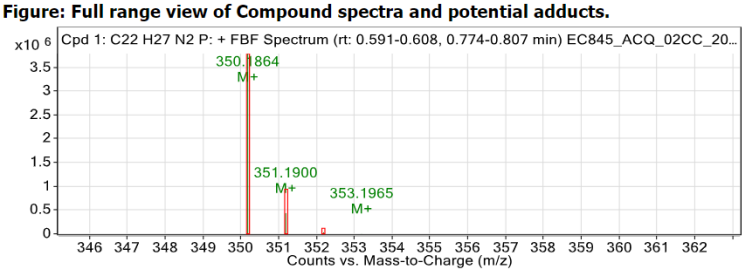

Figure S8. Mass spectrometry analysis of **1**. Top: extracted ion chromatogram for $C_{22}H_{26}N_2P^+$. Bottom: predicted isotope pattern (red) against found isotope pattern (green) for $C_{22}H_{26}N_2P^+$.

3 Characterisation data for 2

3.1 NMR spectroscopy analysis

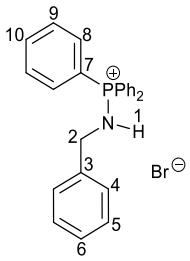

^{1}H NMR (500 MHz, $CDCl_3$, δ (ppm)): 8.76 (s, 1H, H-1), 7.81-7.53 (m, 15H, H-8-10), 7.20-7.10 (m, 5H, H-4-6), 4.29 (m, 2H, H-2)

^{13}C{^{1}H} NMR (126 MHz, $CDCl_3$, δ (ppm)):138.6 (d, *J* = 11.8 Hz, C-3) 134.8 (d, *J* = 11.1 Hz, C-10), 133.9 (d, *J* = 45.0 Hz, C-9), 129.9 (d, *J* = 52.4 Hz, C-8), 128.4 (C-4), 128.3 (C-5) 127.5 (C-6), 122.1 (d, *J* = 334.2 Hz, C-7), 45.7 (C-2)

^{31}P{^{1}H} (202 MHz, $CDCl_3$, δ (ppm)): 38.56

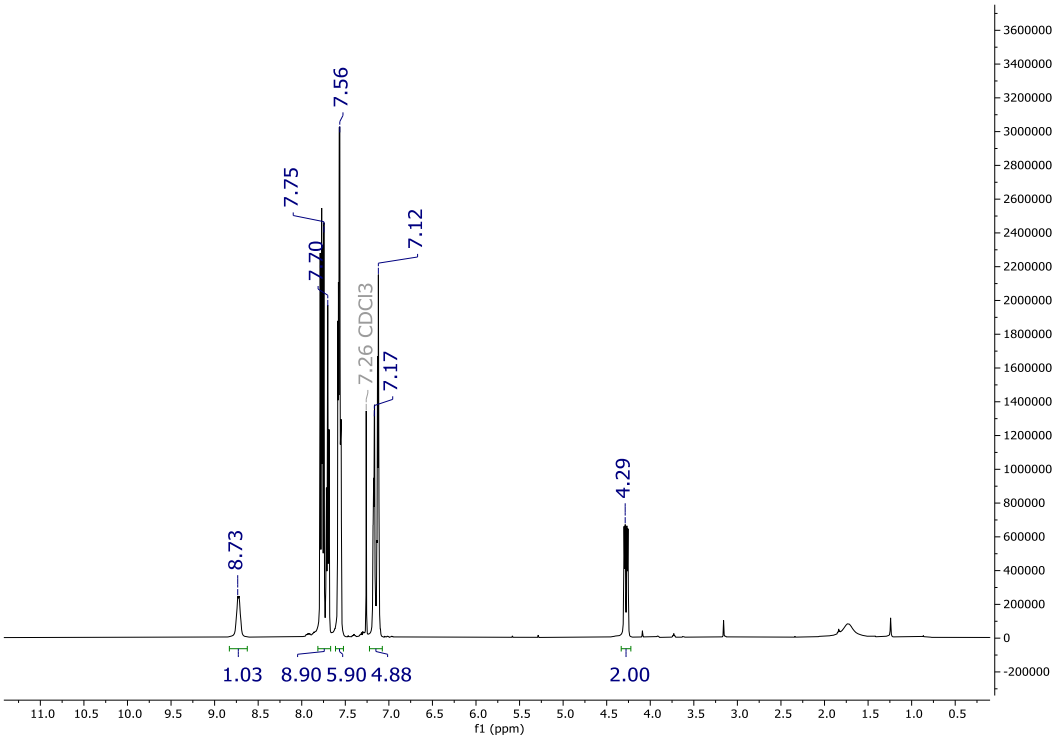

Figure S9. ^{1}H NMR spectrum of **2**.

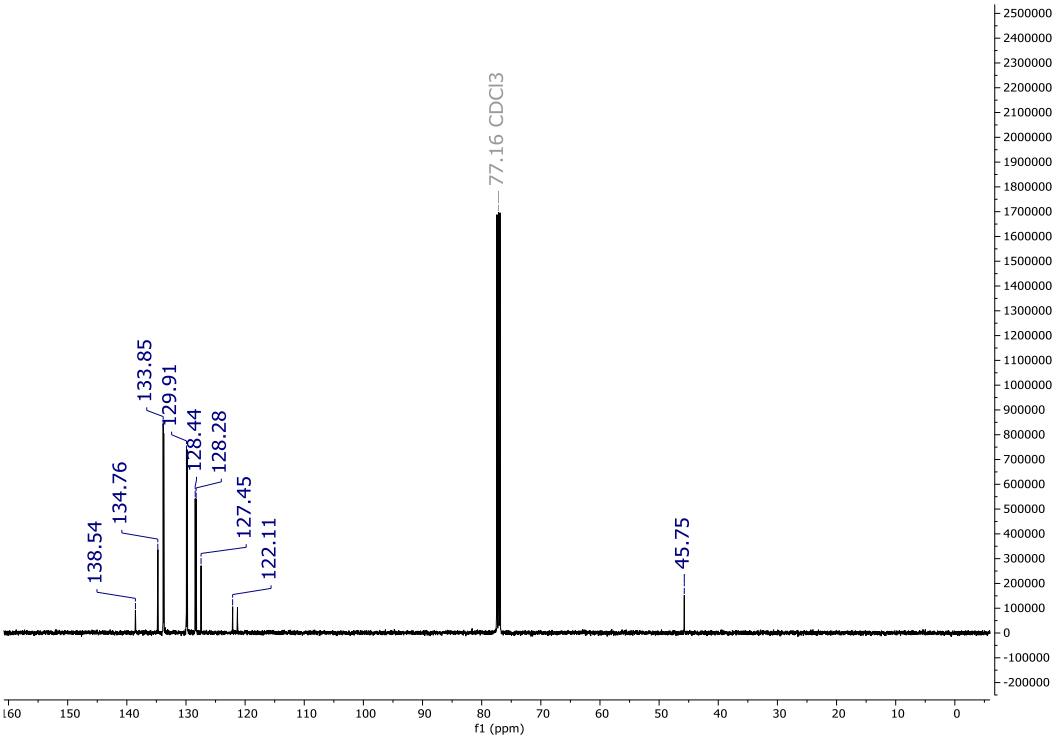

Figure S10. $^{13}C\{^{1}H\}$ NMR spectrum of **2**.

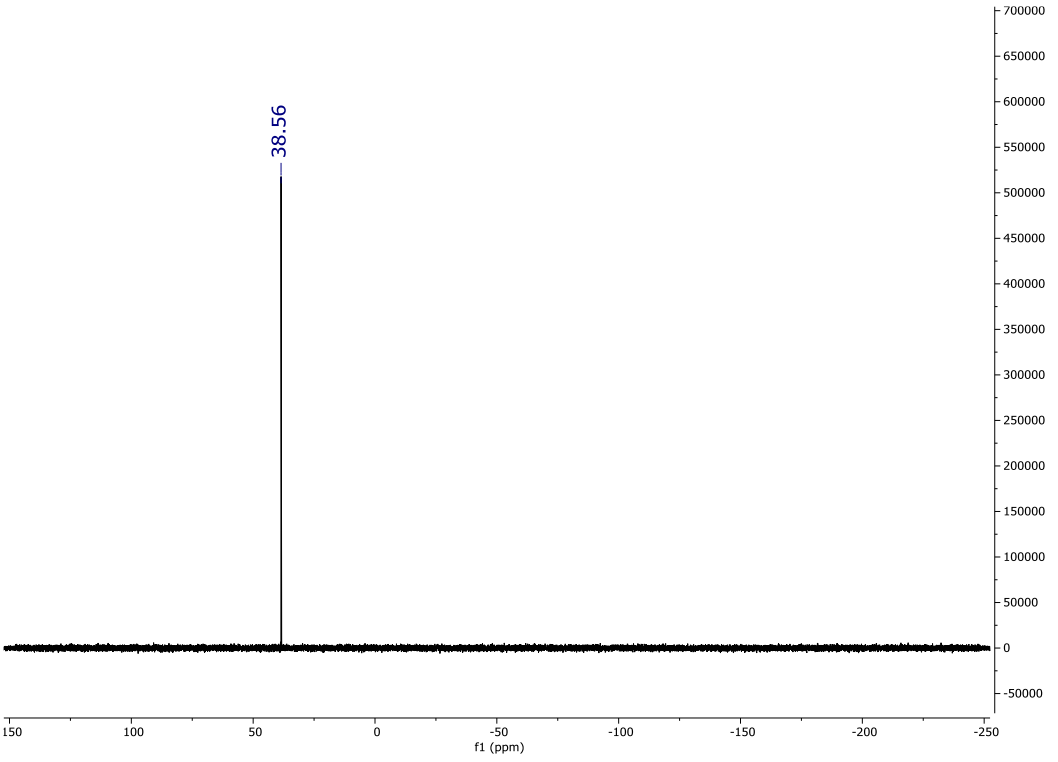

Figure S11. ^{13}P NMR spectrum of **2**.

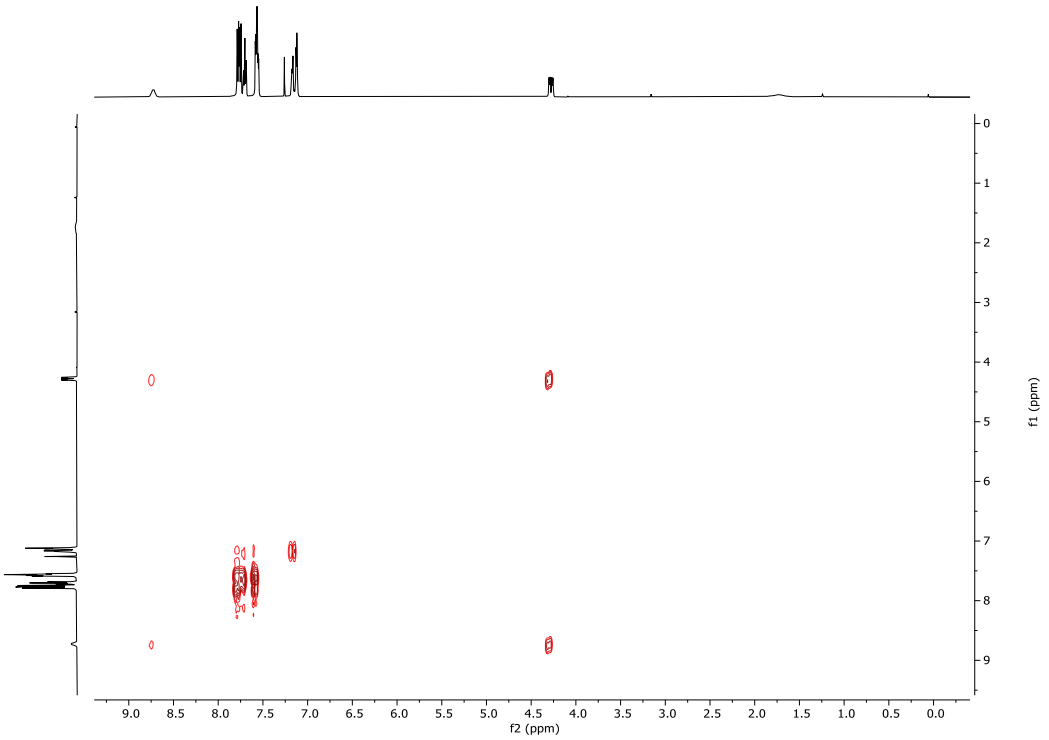

Figure S12. ^{1}H-^{1}H COSY NMR spectrum of **2**.

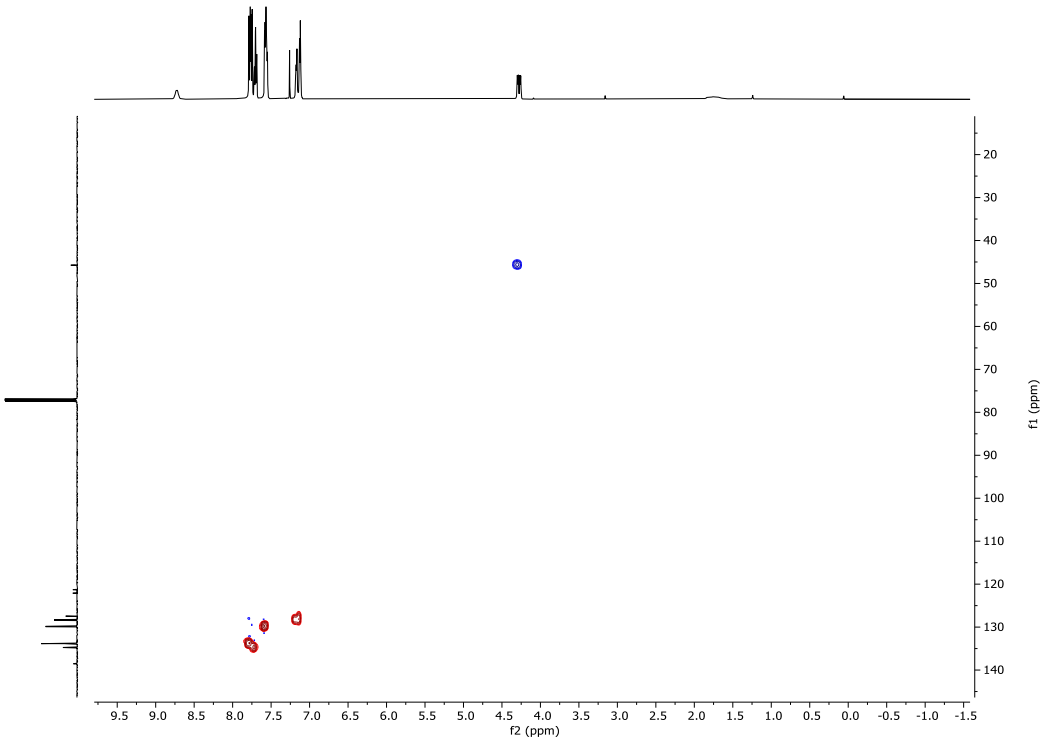

Figure S13. ^{13}C-^{1}H HSQC NMR spectrum of **2**.

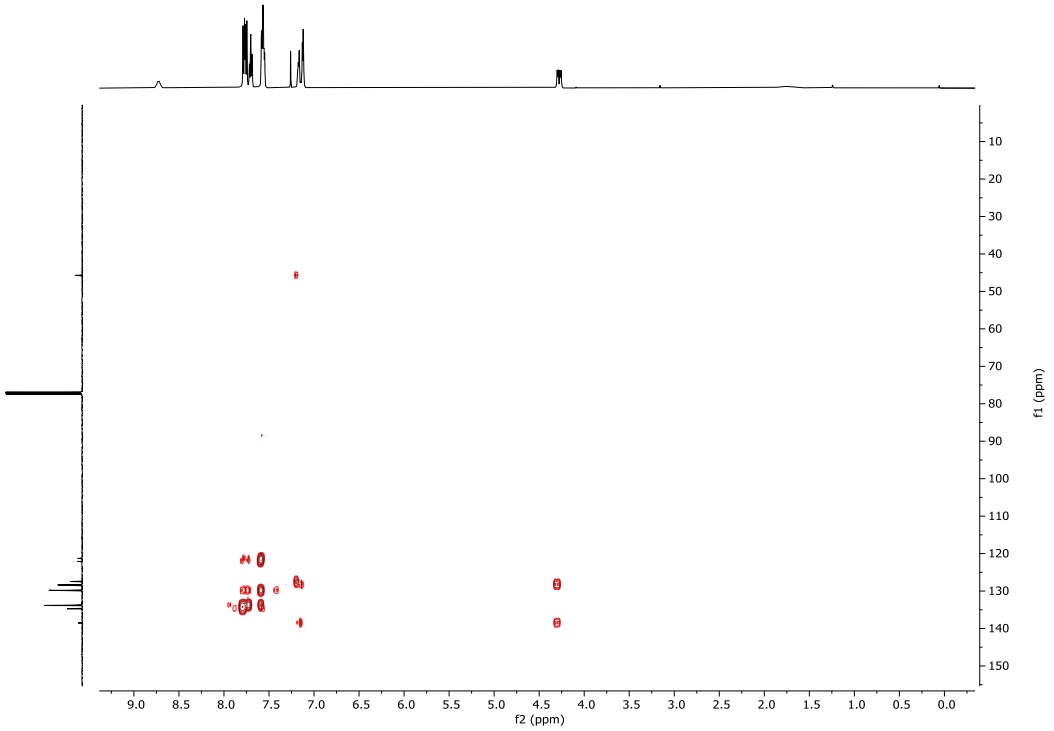

Figure S14. ^{13}C-^{1}H HMBC NMR spectrum of **2**.

3.2 X-ray diffraction analysis

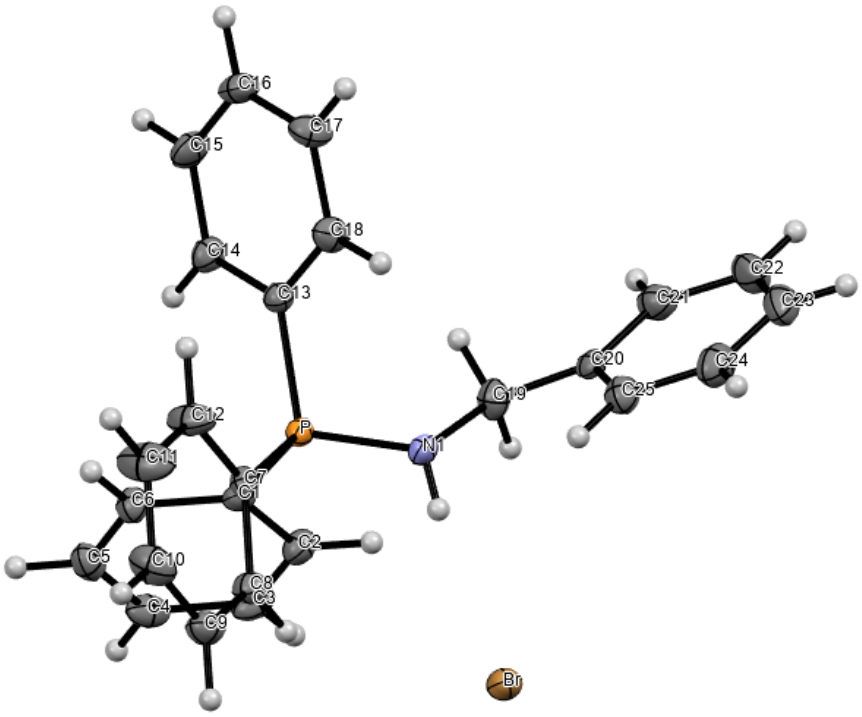

Figure S15. ORTEP drawing of the molecular structure of **2** obtained by X-ray diffraction analysis with thermal ellipsoids at the 50% probability level. CCDC 2374926.

Identification code	e23ab4	
Empirical formula	C_{25} H_{23} Br N P	
Formula weight	448.32	
Temperature	149.9(7) K	
Wavelength	0.71073 Å	
Crystal system	Orthorhombic	
Space group	Pbca	
Unit cell dimensions	a = 11.1188(4) Å	a= 90°.
	b = 18.1495(6) Å	b= 90°.
	c = 21.2078(7) Å	g = 90°.
Volume	4279.7(3) $Å^3$	
Z	8	
Density (calculated)	1.392 Mg/m^3	
Absorption coefficient	2.006 mm^{-1}	
F(000)	1840	
Crystal size	0.520 x 0.450 x 0.210 mm^3	
Theta range for data collection	2.954 to 30.402°.	
Index ranges	-13<=h<=14, -23<=k<=25, -29<=l<=29	
Reflections collected	38624	
Independent reflections	5981 [R(int) = 0.0507]	
Completeness to theta = 25.242°	99.8 %	
Absorption correction	Semi-empirical from equivalents	
Max. and min. transmission	1.00000 and 0.79427	
Refinement method	Full-matrix least-squares on F^2	
Data / restraints / parameters	5981 / 0 / 257	
Goodness-of-fit on F^2	1.015	
Final R indices [I>2sigma(I)]	R_1 = 0.0397, wR_2 = 0.0710	
R indices (all data)	R_1 = 0.0717, wR_2 = 0.0810	
Extinction coefficient	n/a	
Largest diff. peak and hole	0.432 and -0.388 $e.Å^{-3}$	

4 Characterisation data for 4

4.1 NMR spectroscopy analysis

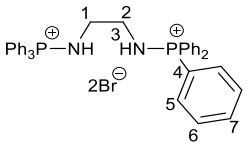

^{1}H NMR (500 MHz, $CDCl_3$, δ (ppm)): 7.82-7.61 (m, 30H, H-5-7), 3.45 (m, 4H, H-1, H-2), 2.75 (s, 2H, H-3)

^{13}C{^{1}H} NMR (126 MHz, $CDCl_3$, δ (ppm)):134.9 (d, *J* = 2.9 Hz, C-7) 133.9 (d, *J* = 11.0 Hz, C-6), 130.2 (d, *J* = 13.3 Hz, C-5), 120.9 (d, *J* = 103.2 Hz, C-4), 42.8 (C-1, C-2)

^{31}P{^{1}H} (202 MHz, $CDCl_3$, δ (ppm)): 38.29

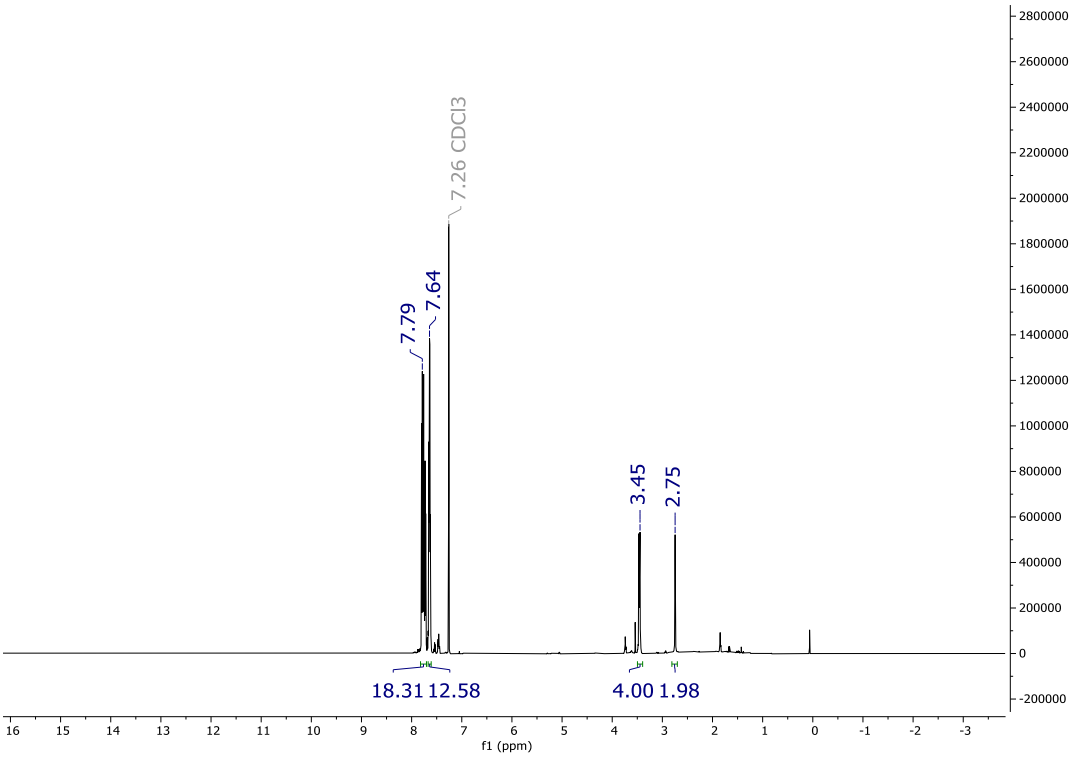

Figure S16. ^{1}H NMR spectrum of **4**.

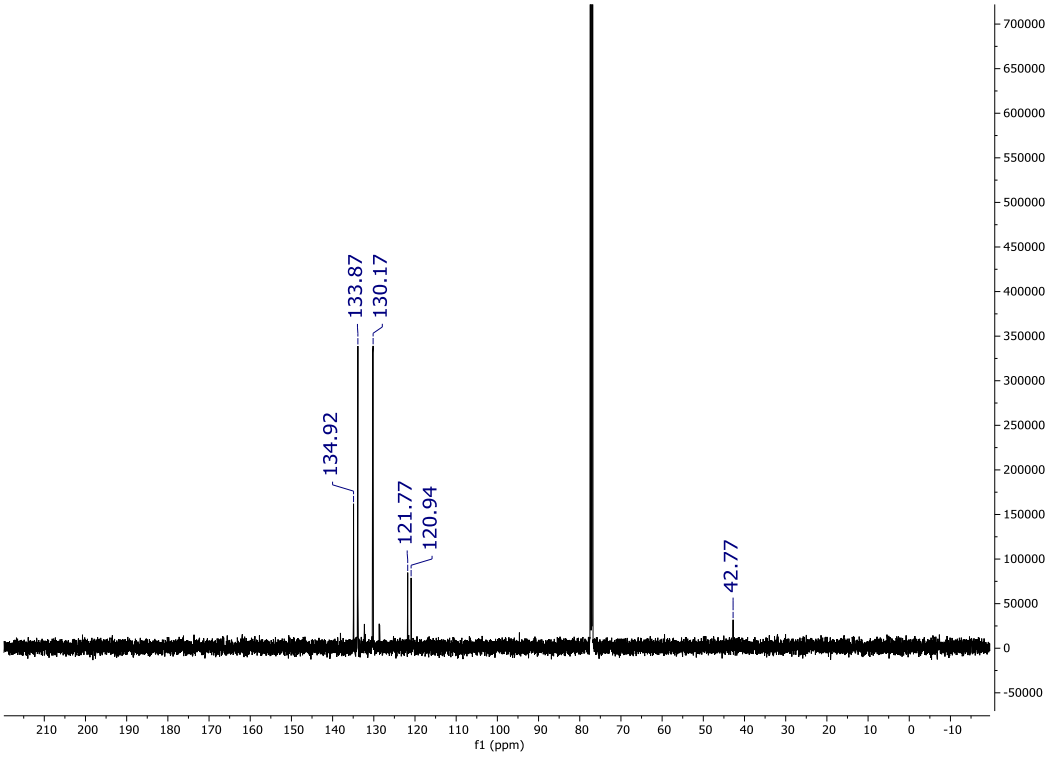

Figure S17. $^{13}C\{^{1}H\}$ NMR spectrum of **4**.

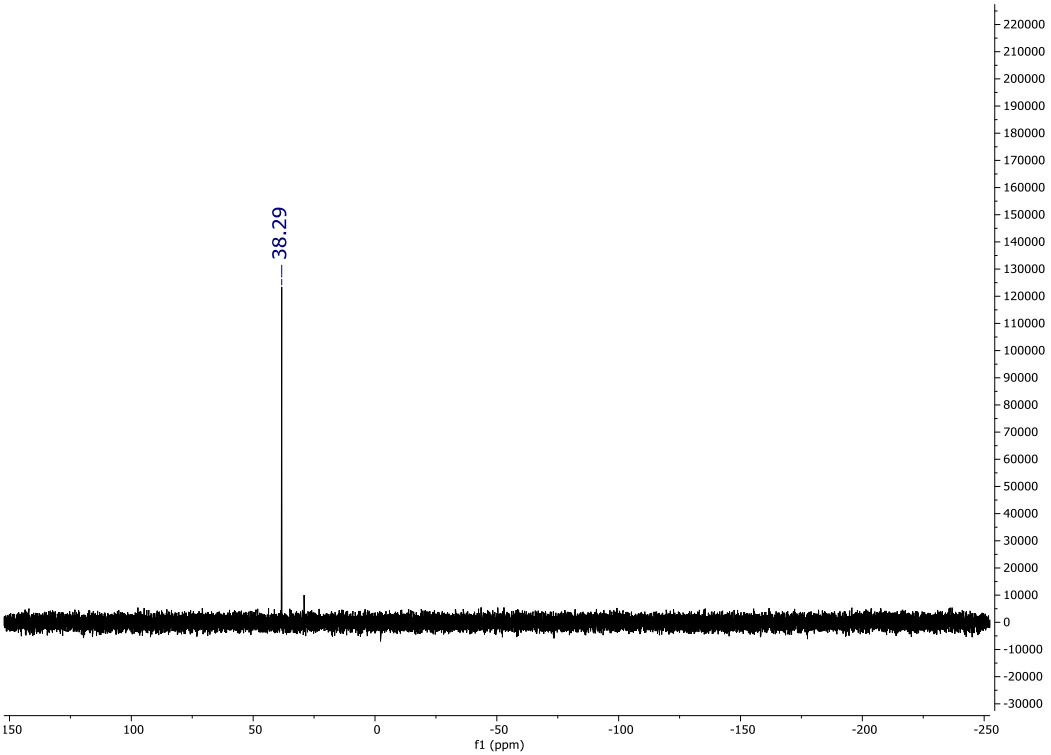

Figure S18. $^{31}P\{^{1}H\}$ NMR spectrum of **4**.

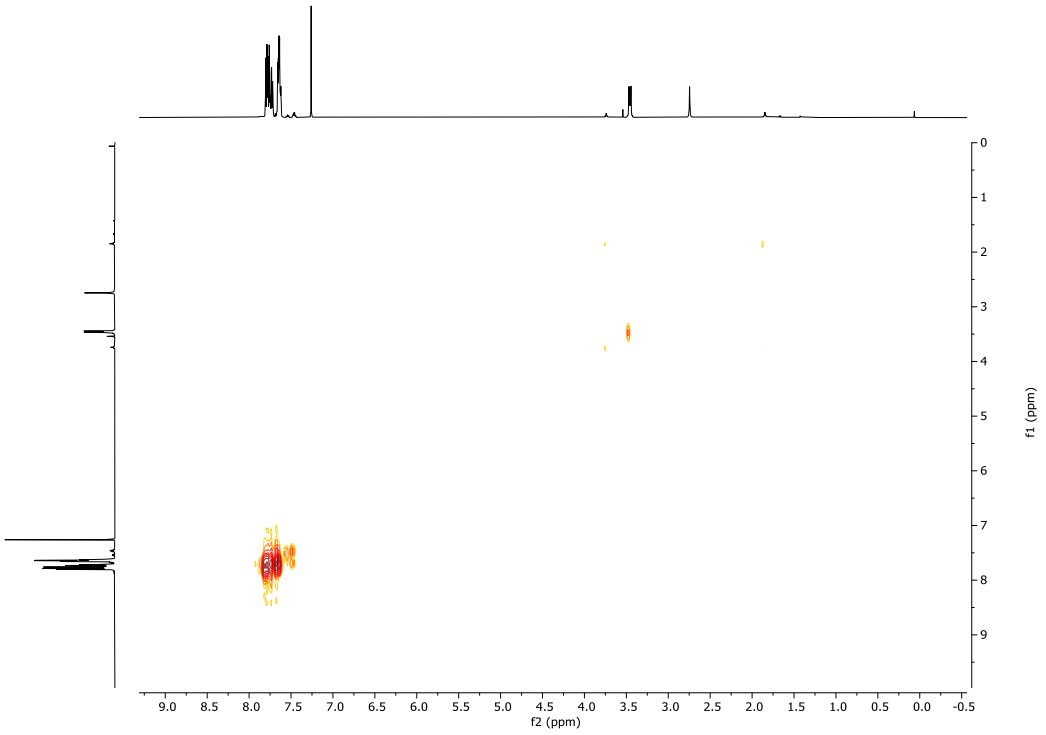

Figure S19. ^{1}H COSY NMR spectrum of **4**.

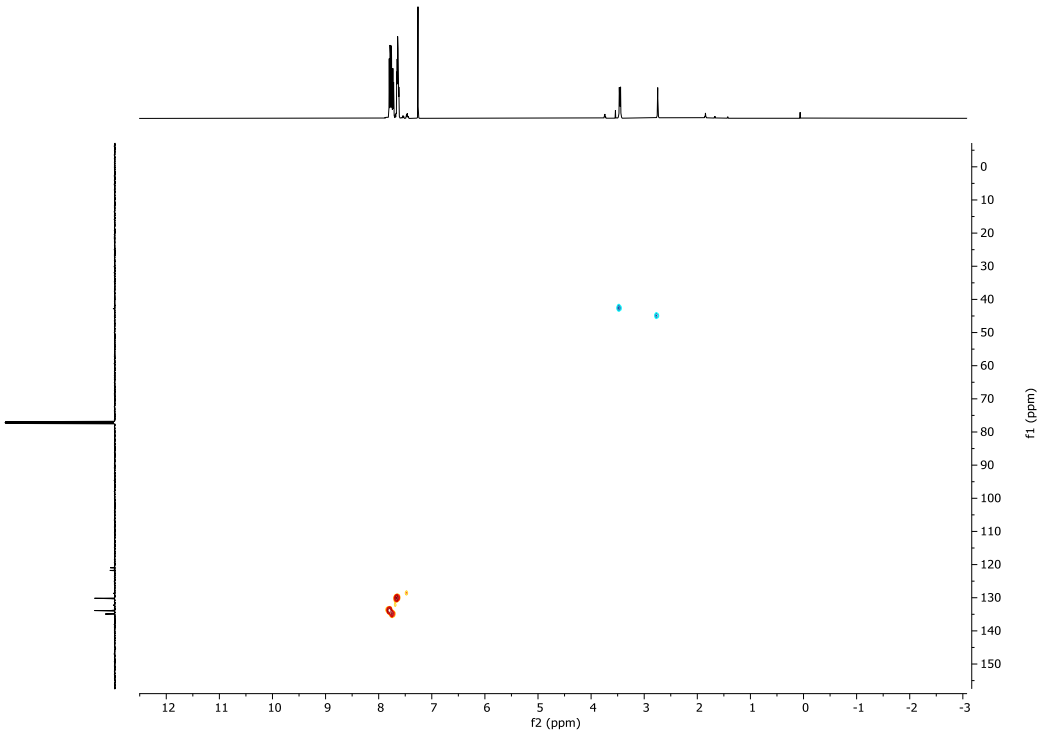

Figure S20. ^{13}C{^{1}H}-^{1}H HSQC NMR spectrum **4**.

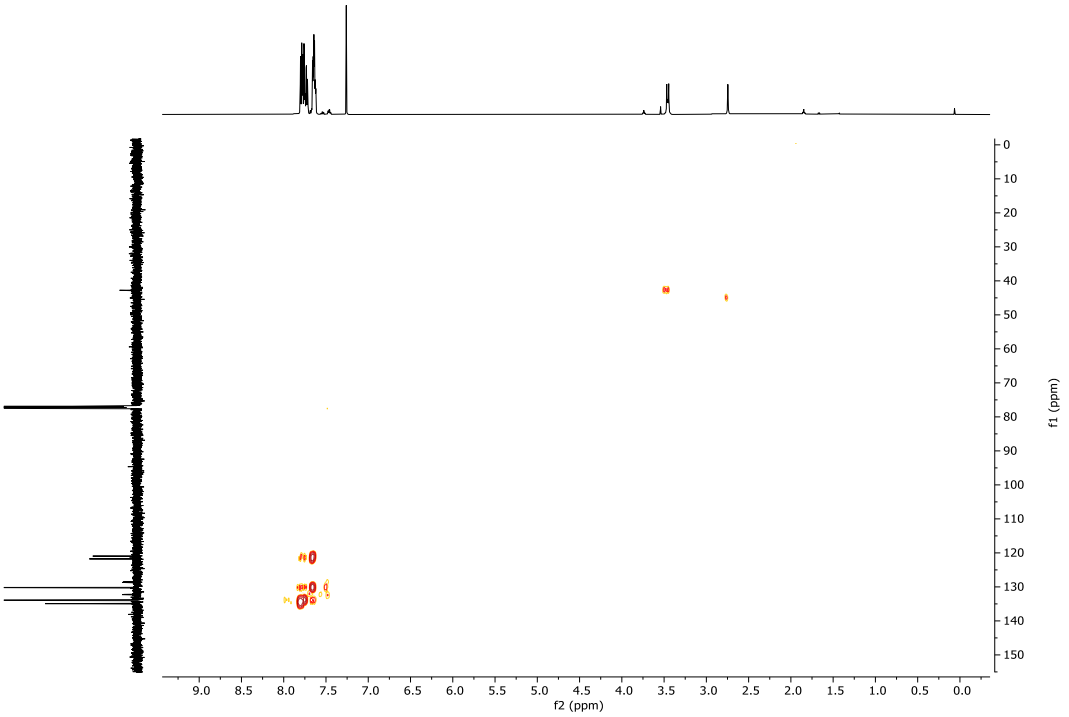

Figure S21. $^{13}C\{^{1}H\}$-^{1}H HMBC NMR spectrum **4**.

5 NMR analysis of acid/base addition to 1

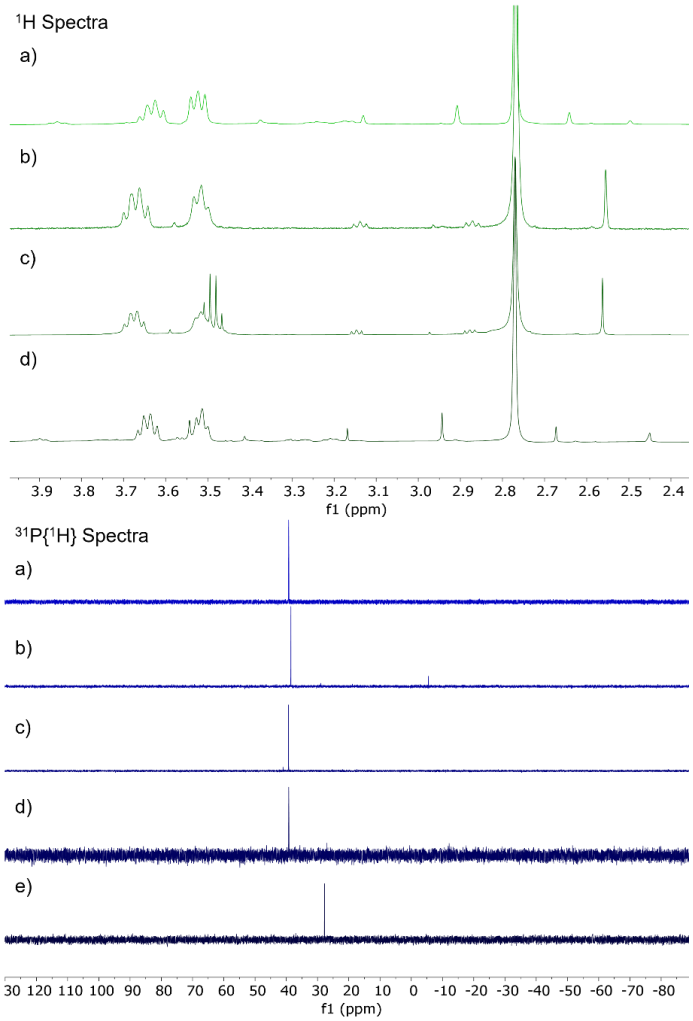

Figure S22. ^{1}H NMR spectra (500 MHz, $CDCl_3$) and $^{31}P\{^{1}H\}$ NMR spectra (162 MHz-$CDCl_3$), of a) **1** synthesised without base, b) **1** synthesised with DABCO, c) a and b combined, d) a with $HCl_{(ether)}$ added and e) a with KOH added.

Repeating the synthesis of **1** with the addition of DABCO resulted in no change in the resulting shift at 39.00 ppm as observed by $^{31}P\{^{1}H\}$ NMR spectroscopy. Attempts to deprotonate an hypothetical quaternary ammonium cation by addition of 1 equivalent of KOH resulted in the formation of PPh_3O, confirmed by $^{31}P\{^{1}H\}$ NMR analysis (**Figure S22**). Alternatively, efforts to protonate the tertiary amine of **1** by addition of 1 equivalent of HCl (2 mol L^{-1} in Et_2O) affected no change in the $^{31}P\{^{1}H\}$ NMR spectra (**Figure S22**). ^{1}H NMR analysis of the combined products from the synthesis with and without base indicated the presence of only one species (**Figure S22**).

6 Polymer characterisation and polymerisation data

6.1 NMR spectroscopy analysis of ROCOP of CHO/PA

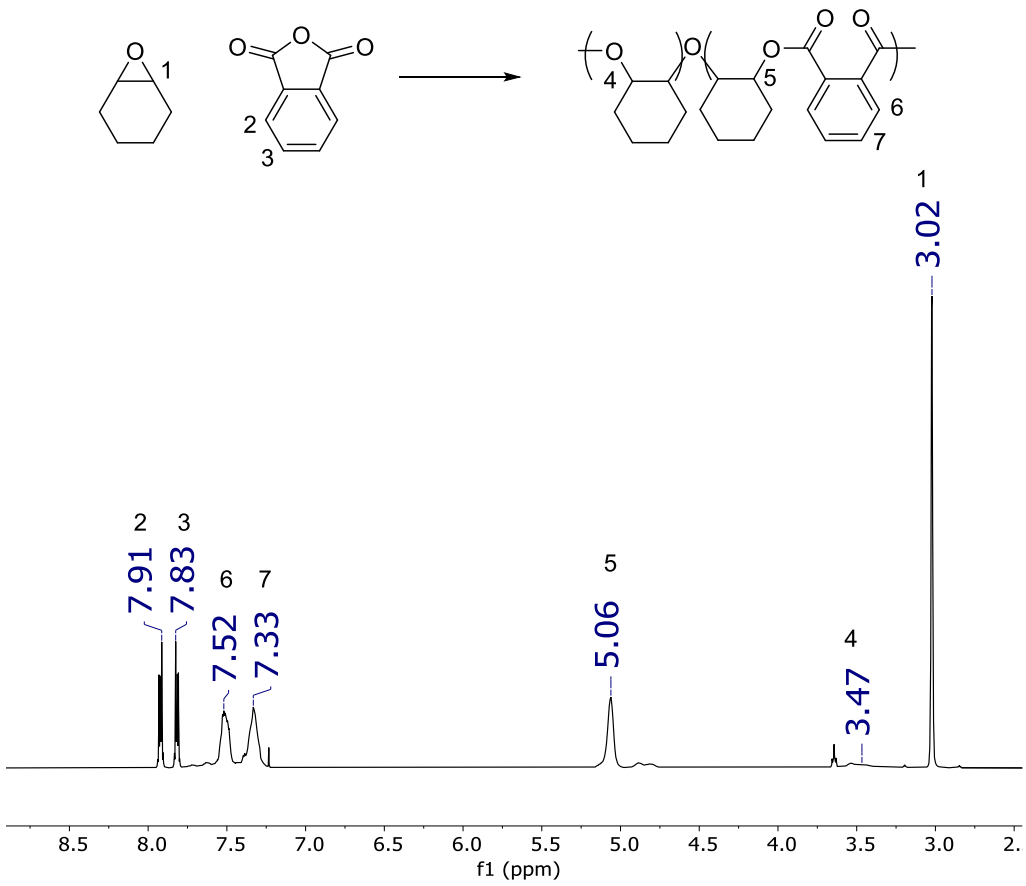

Figure S23. ^{1}H NMR spectrum (500 MHz, $CDCl_3$) of crude reaction mixture from a typical ROCOP of CHO/PA catalysed by **1**, with assignments of signals from residual CHO and PA, polyester and ether linkages defects.

6.2 MALDI-ToF mass spectrometry analysis of poly(CHO-*alt*-PA) made using 1 as catalyst

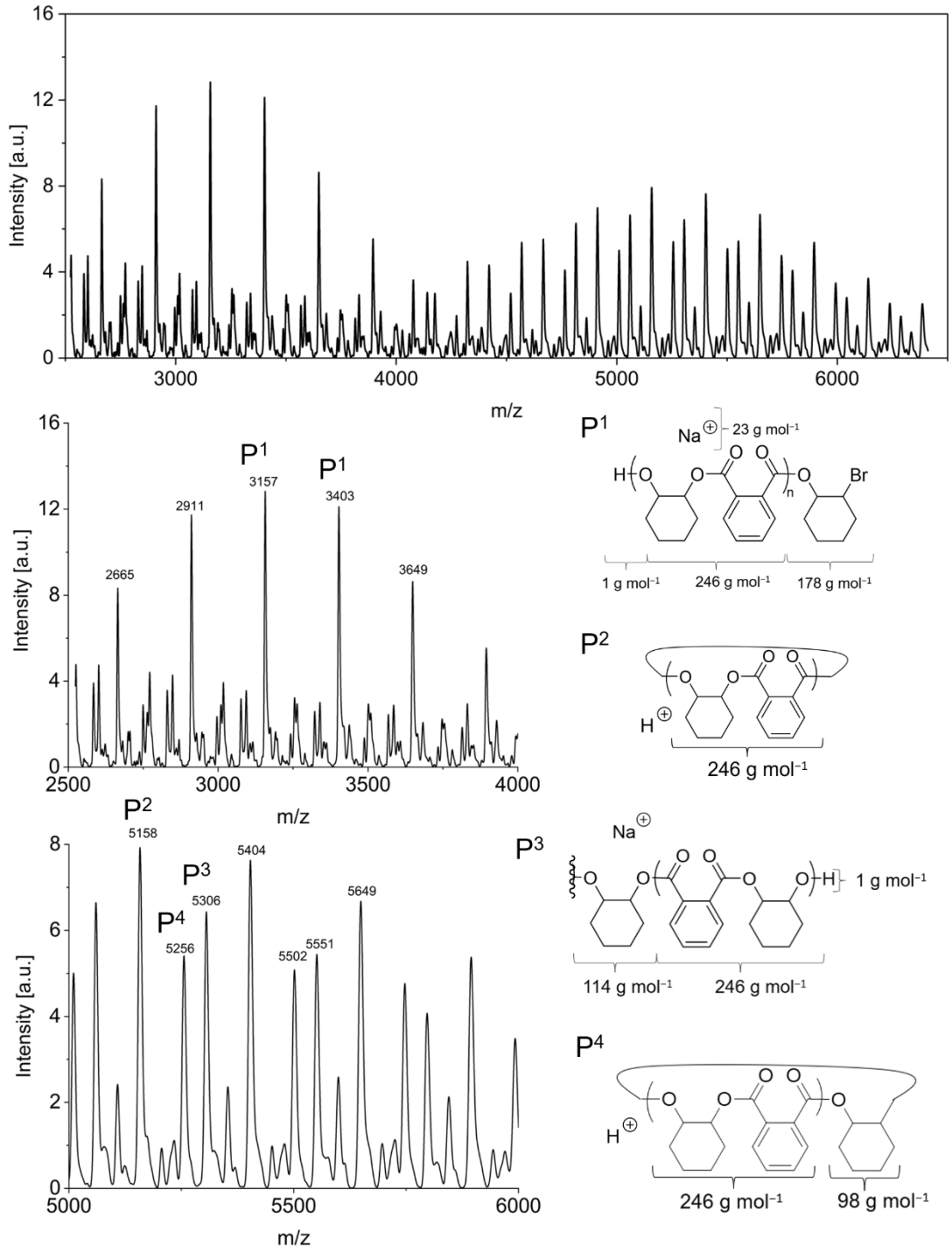

Figure S24. Top, full MALDI-ToF spectrum showing bimodal nature. Bottom, zoomed in MALDI-ToF spectrum showing detected series. The primary, lower *m/z* series is assigned as linear polymer species with CHO-Br chain ends (P1), detected as Na^+ adducts. The higher *m/z* minor series were assigned as: P2 and P4, cyclic polymer species and P3, linear polymer species grown from cyclohexane diol, detected as Na^+ adducts.

6.3 Monitoring of $M_{n,SEC}$ and $Đ_M$ against PA monomer conversion

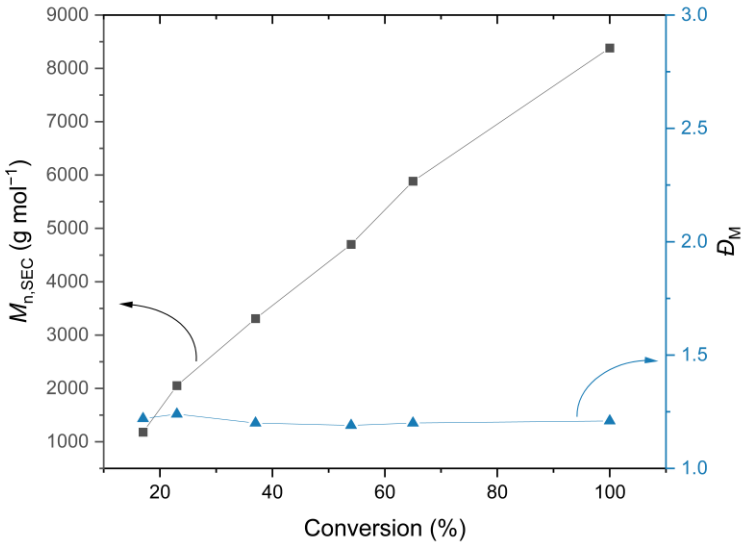

Figure S25. Conversion of PA (determined by ^{1}H NMR spectroscopy) *vs* $M_{n,SEC}$ (black, square) and $Đ_M$ (blue, triangle) in the ROCOP of CHO with PA at 120 °C with $[CHO]_0$:$[PA]_0$:$[\mathbf{1}]_0$ loadings of 200:100:1 $[CHO]_0$ = 5.8 mol L^{-1} without solvent.

6.4 Size-Exclusion Chromatogram of poly(CHO-*alt*-PA) derived from 1

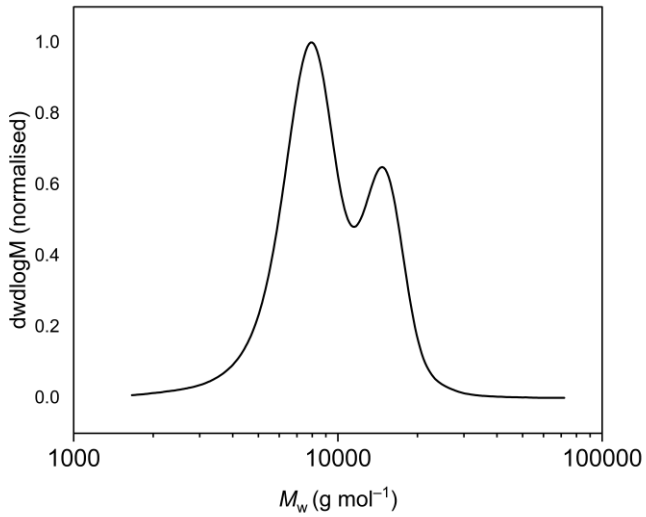

Figure S26. SEC chromatogram (THF eluent) of poly(CHO-*alt*-PA) at 100% conversion of PA ($M_{n,SEC}$ = 8,400 g mol^{-1}, $Đ_M$ = 1.22) with $[CHO]_0$:$[PA]_0$:$[\mathbf{1}]_0$ loadings of 200:100:1 $[CHO]_0$ = 5.8 mol L^{-1} without solvent.

6.4 $^{31}P\{^{1}H\}$ NMR spectroscopy monitoring of CHO/PA ROCOP catalysed by 1

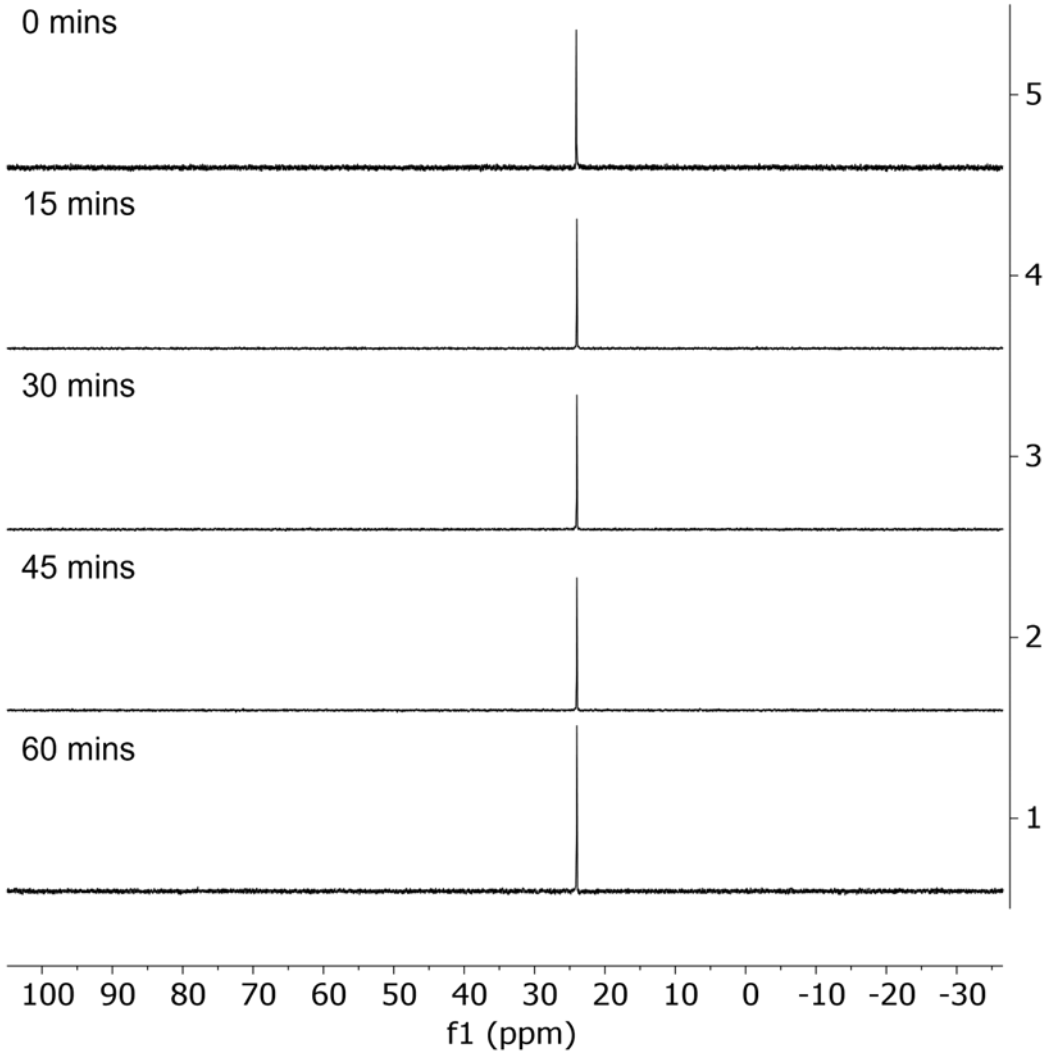

Figure S27. *in-situ* $^{31}P\{^{1}H\}$ NMR reaction monitoring of CHO/PA ROCOP catalysed by **1**, using a $[PA]_0$:$[1]_0$ ratio of 50:1 in a large excess of CHO (over twice the amount of PA) at 120 °C.

6.5 Kinetics of CHO/PA ROCOP catalysed by 1

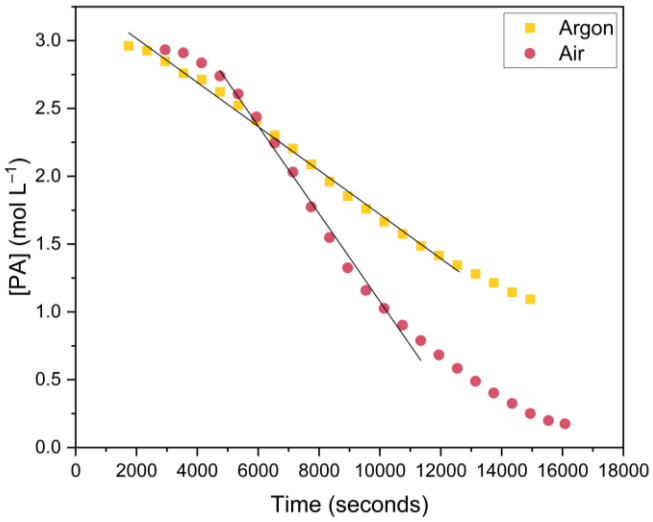

Figure S28. Plot of $[PA]_t$ *vs* Time (seconds) at $[\mathbf{1}]_0$:$[PA]_0$:$[CHO]_0$ = 1:400:800 at 120 °C. Data acquired using *in-situ* FTIR spectroscopy, monitoring the absorption intensity at 1783 cm^{-1} (corresponding to the $\nu_{C=O}$ vibration in PA) under an argon atmosphere and in air.

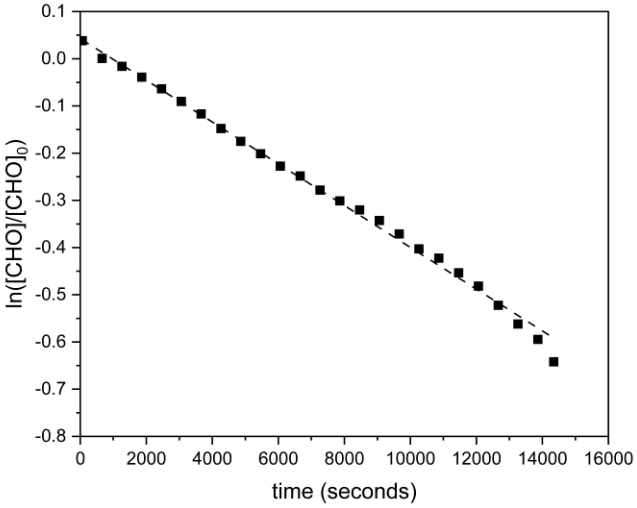

Figure S29. Plot of $\ln([CHO]_t/[CHO]_0)$ *vs* time, revealing a linear relationship and hence a first-order dependence of the rate on [CHO]. Conditions: $[\mathbf{1}]_0$:$[PA]_0$:$[CHO]_0$ = 1:400:800, T = 120 °C. [CHO] was calculated by subtracting the growth of the $\nu_{C=O}$ vibration at 1722 cm^{-1} in poly(CHO-*alt*-PA), from $[CHO]_0$.

7 Computational Modelling

7.1 Free enthalpy reaction profiles

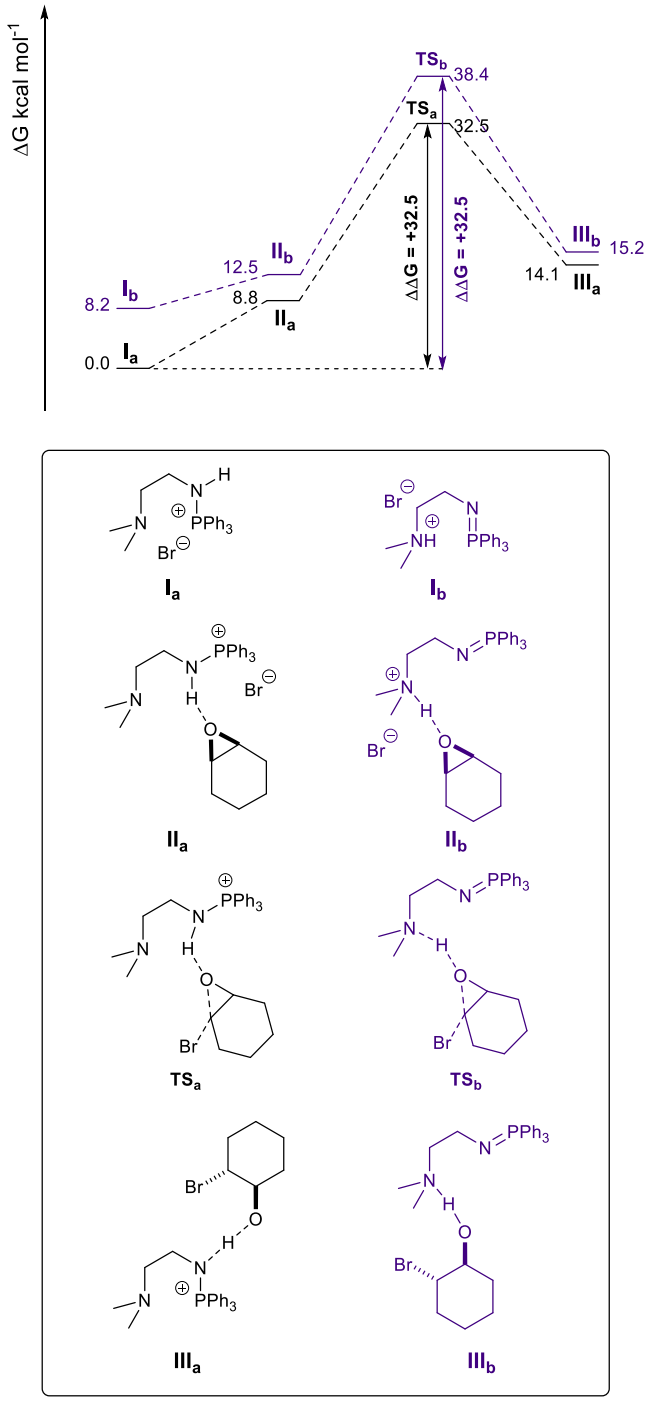

Figure S30. DFT computed free enthalpy diagram for the ring-opening of CHO by **1** (initiation step of ROCOP). Protocol: ωb97xD/6-311++G(d,p) and 6-31+G(d) /cpcm=THF/393.15K. Free enthalpies given in kcal mol^{-1}.

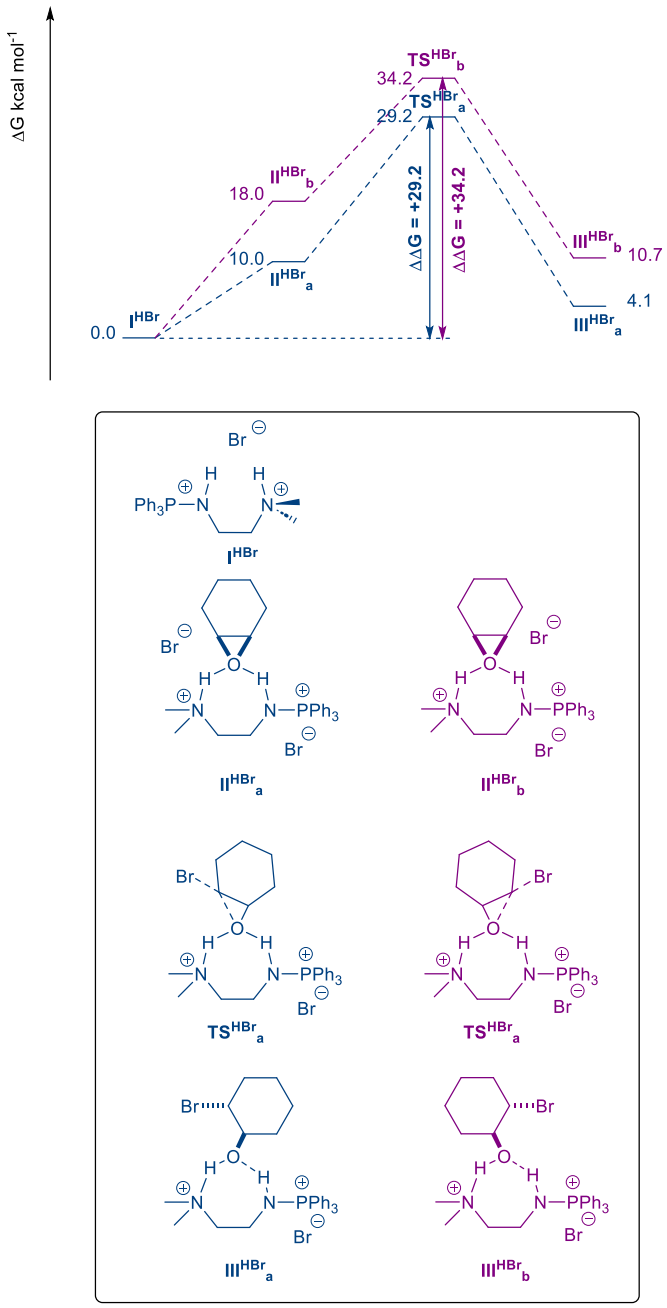

Figure S31. DFT computed free enthalpy diagram for the ring-opening of CHO by **1·HBr** (initiation step of ROCOP from a putative dicationic species). Protocol: ωb97xD/6-311++G(d,p) and 6-31+G(d) /cpcm=THF/393.15K. Free enthalpies given in kcal mol^{-1}.

7.2 Computed free enthalpies

Table S1. Computed free enthalpies of intermediates and transition states for the first ring-opening of cyclohexene oxide (CHO) by **1** and **1·HBr**.

Structure	G (Hartree)[a]	ΔΔG (kcal mol^{-1})[a]	G (Hartree)b	ΔΔG (kcal mol^{-1})[b]
CHO	-309.679082		-309.684886	
I_a	-3878.475129	0	-3878.494892	0
I_b	-3878.462026	+8.2	-3878.481888	+8.2
Reference for CHO opening by **1** (I_a +CHO)	-4188.154211	0	-4188.179778	0
II_a	-4188.1432	+6.9	-4188.165792	+8.8
II_b	-4188.137931	+10.2	-4188.159815	+12.5
TS_a	-4188.104309	+31.3	-4188.128013	+32.5
TS_b	-4188.095777	+36.7	-4188.118625	+38.4
III_a	-4188.13437	+12.4	-4188.157305	+14.1
III_b	-4188.132831	+13.4	-4188.155592	+15.2
I^{HBr}	-6453.297478		-6453.317012	
Reference for CHO opening by **1·HBr** (I_a +CHO)	-6762.97656	0	-6763.001898	0
$II^{HBr}{}_a$	-6762.963796	+8.0	-6762.985939	+10.0
$II^{HBr}{}_a$	-6762.951686	+15.6	-6762.973158	+18.0
$TS^{HBr}{}_a$	-6762.933025	+27.3	-6762.955327	+29.2
$TS^{HBr}{}_b$	-6762.92456	+32.6	-6762.947313	+34.2
$III^{HBr}{}_a$	-6762.973668	+1.8	-6762.995293	+4.1
$III^{HBr}{}_b$	-6762.962873	+8.6	-6762.984826	+10.7

Protocol: ωb97xD/6-311++G(d,p) and 6-31+G(d)/cpcm=THF. [a] Default temperature = 298.15 K, concentration = 1.0 mol L^{-1} . [b] Goodvibes correction applied at 393.15 K and concentration = 0.0127 mol L^{-1} (5.07 mol L^{-1} for [CHO])

8. References

[1] Frisch, M. J.; Trucks, G. W.; Schlegel, H. B.; Scuseria, G. E.; Robb, M. A.; Cheeseman, J. R.; Scalmani, G.; Barone, V.; Petersson, G. A.; Nakatsuji, H.; Li, X.; Caricato, M.; Marenich, A. V.; Bloino, J.; Janesko, B. G.; Gomperts, R.; Mennucci, B.; Hratchian, H. P.; Ortiz, J. V.; Izmaylov, A. F.; Sonnenberg, J. L.; Williams; Ding, F.; Lipparini, F.; Egidi, F.; Goings, J.; Peng, B.; Petrone, A.; Henderson, T.; Ranasinghe, D.; Zakrzewski, V. G.; Gao, J.; Rega, N.; Zheng, G.; Liang, W.; Hada, M.; Ehara, M.; Toyota, K.; Fukuda, R.; Hasegawa, J.; Ishida, M.; Nakajima, T.; Honda, Y.; Kitao, O.; Nakai, H.; Vreven, T.; Throssell, K.; Montgomery Jr., J. A.; Peralta, J. E.; Ogliaro, F.; Bearpark, M. J.; Heyd, J. J.; Brothers, E. N.; Kudin, K. N.; Staroverov, V. N.; Keith, T. A.; Kobayashi, R.; Normand, J.; Raghavachari, K.; Rendell, A. P.; Burant, J. C.; Iyengar, S. S.; Tomasi, J.; Cossi, M.; Millam, J. M.; Klene, M.; Adamo, C.; Cammi, R.; Ochterski, J. W.; Martin, R. L.; Morokuma, K.; Farkas, O.; Foresman, J. B.; Fox, D. J. *Gaussian 16 Rev. C.01*, Wallingford, CT, 2016.

[2] Chai, J.-D.; Head-Gordon, M., Long-range corrected hybrid density functionals with damped atom–atom dispersion corrections. *Phys. Chem. Chem. Phys.* **2008,** *10* (44), 6615-6620.

[3] Chai, J.-D.; Head-Gordon, M., Optimal operators for Hartree–Fock exchange from long-range corrected hybrid density functionals. *Chem. Phys. Lett.* **2008,** *467* (1), 176-178.

[4] Luchini, G.; Alegre-Requena, J. V.; Funes-Ardoiz, I. and Paton, R.S. Goodvibes: automated thermochemistry for heterogeneous computational chemistry data. *F1000Research*, **2020**, *9*, 291.